Electronic Supplementary Material (ESI) for Nanoscale Horizons.

Chiroptically Active Quantum Nanonails

Finn Purcell-Milton[1]*, Vera A. Kuznetsova[1], Xue Bai[1], Áine Coogan[1], Marina Martínez-Carmona, Jorge A. Garcia[2], Louise Bradley[2], Yurii K. Gun'ko[1]*

[1] *School of Chemistry, CRANN and AMBER Research Centres, Trinity College Dublin, Dublin, Ireland.*

[2] *School of Chemical & BioPharmaceutical Sciences, Technological University Dublin, Grangegorman, Dublin, Ireland.*

[3] *Departamento de Didáctica de las Ciencias Experimentales, Universidad de Murcia, 30100 Murcia, Spain.*

[4] *School of Physics, Trinity College Dublin, Dublin 2, Ireland.*

Emails: finn.purcellmilton@tudublin.ie, kuznetsv@tcd.ie, igounko@tcd.ie

Supporting Information

Index

I. Materials and Methods

Chemicals:

All chemical reagents were used as purchased without further purification. Acetone (HPLC), chloroform (HPLC), cysteine (L and D) 1-dodecanethiol (98%), hexylphosphonic acid (HPA , 95%), hexane (HPLC), hydrochloric acid (37%), methanol (HPLC), oleic acid (OA, 90%), 1-octadecene (ODE, 90%), octadecylphosphonic acid (ODPA, 97%), oleylamine (98%), potassium hydroxide (85%), selenium (99.99%), sulphur (99.998%), tetradecylphosphonic acid (TDPA, 97 %); toluene (HPLC), trioctylphosphine (TOP, 97%), trioctylphosphine oxide (TOPO, 99%) were purchased from Sigma-Aldrich. Cadmium oxide (99.995%) were purchased from Alfa Aesar.

Zinc blende (zb)-CdSe QD Synthesis

This synthesis was carried out following a modified published procedure. [1,2] Firstly a 0.5 M $Cd(oleate)_2$ oleic acid solution was produced, by adding 1.284 g of CdO to 20 ml of oleic acid in 3-neck 100 ml flask. The resultant solution was degassed at 100 °C for 20 minutes, and then heated to 240 °C and held at this temperature for 20 minutes. The solution was then allowed to cool to 100 °C and subjected to vacuum for a further hour to remove volatile components. Following this, the reaction vessel was switched to an argon atmosphere and allowed to cool to room temperature. Following this, the Se injection solution was prepared. Firstly 1.5 ml of 1 M TOP-Se (0.1184 g in 1.5 ml of TOP), 1.5 ml of oleylamine, 1 g of TDPA (heated until the solution became clear) and 2 ml of ODE were added to a 10 ml round-bottomed flask under an argon atmosphere and heated to 165 °C. 2 ml of 0.5 M $Cd(oleate)_2$ in oleic acid was mixed with 8 ml of ODE and introduced into a 100 ml three-neck flask. The mixture was degassed at 70 °C under vacuum for 1 h. Under argon flux, the temperature was increased to the injection temperature of 240 °C before injecting a mixture of the Se injection solution. Upon injection, the reaction was then maintained at the injection temperature for variable growth time (0 - 5 minutes) and then removed from the heat source. After cooling to 80 °C, 30 ml ethanol was added to the solution to prevent solidification of the product. The sample was cooled at room temperature and more ethanol (60 ml) was added before centrifugation at 9000 RPM g for 4 min. The supernatant was discarded and the pellet containing CdSe nanocrystals and TDPA was suspended in 10 ml hexane and sonicated for 5 min. This turbid solution was centrifuged for 5 min at room temperature. The clear supernatant containing the QDs was precipitated one more time with 90 ml ethanol and centrifuged. The pellet containing the QDs was suspended in 10 ml hexane.

CdSe/CdS NN Synthesis

This synthesis was carried out following a modified published procedure. [3] Firstly, the CdSe seed injection solution was prepared. A mixture of S, TOP, and CdSe seeds was prepared by firstly dissolving a predetermined amount of S (0.021 mg) in 1.8 ml of TOP at 50 °C under an inert atmosphere before adding the appropriate CdSe seed stock solution. Following this, the CdSe-seeded CdS heterostructures were synthesized via the seeded growth approach. Briefly, 6.625 g of TOPO, 0.13 g of CdO, and ODPA (0.35 g), OA (1.25 mL) were degassed at 150 °C for 1.5 h in a 100 mL three-neck round-bottomed flask. The reaction mixture was then heated to 350 °C under inert atmosphere, at which point the solution turned from reddish-brown to colourless. Upon reaching the desired injection temperature of 350 °C, 2.25 ml of TOP was added, and the temperature was allowed to recover to 350 °C before the mixture of S, TOP, and CdSe was swiftly injected. The temperature was again allowed to recover to 350 °C and the anisotropic CdS shell was grown at this temperature for 10 minutes. The vessel was then removed from the heating mantle, and the solution was allowed to cool to room temperature. As-synthesized CdSe-seeded CdS nanorods were then processed by repeated cycles of

precipitation in methanol and redispersed in toluene. The material was then crashed out of solution using MeOH. Following this, the NPs were dissolved in toluene and centrifuged at 9,000 RPM for 10 minutes, to ensure removal of the excess ligands left from the synthesis in the supernatant, just giving the cleaned NNs as a pellet. The pellet was re-dissolved in toluene, and repeated if further cleaning was required.

Ligand Exchange of NN with Chiral Cysteine Molecules

Cysteine ligand exchange was carried out using the previously reported method [4] with some modifications. Briefly, 750 µL of NNs in chloroform with the UV-Vis absorbance at 400 nm adjusted to 1 for convenience in further measurements, were precipitated with methanol (750 µL), centrifuged, and redissolved in chloroform (750 µL). Then 75 µL of a cysteine hydrochloride solution in methanol (0.27 mM) was added to the QD chloroform solution, shaken, and left for 2 minutes. Following this, 750 µL of an aqueous 0.01 M KOH solution was added, therefore adjusting the pH to 12 and forming a bilayer solution. The layers were then mixed by gentle inversions multiple times until the majority of the QDs have transferred to the aqueous layer. The sample was then centrifuged in order to fully separate the layers and remove aggregates (15 000 RPM, 1 min). Finally, the aqueous layer was extracted and stored in a refrigerator at approximately 2-5 °C. For the study of the influence of cysteine concentration on the CD signal, a proportionally smaller volume of cysteine solution in methanol was added or, for higher concentrations, an appropriate amount of cysteine was additionally added to the aqueous solution of NNs after ligand exchange.

Monolayer NN Measurements

NN monolayers were fabricated on quartz substrates using a Layer-by-Layer (LBL) electrostatic assembly technique. [5, 6, 7, 8] The QDs were deposited on a buffer layer of two polyelectrolyte (PE) bilayers of poly(sodium 4-styrene sulfonate) (PSS) and poly(diallyldimethylammonium chloride) (PDDA) on a quartz surface. The polyelectrolyte bilayer forms a strong and homogenously charged surface for the adsorption of the NNs. Four samples with different concentrations were obtained by varying the concentration of NN QDs in solution. The immersion time was kept constant. The concentration of the monolayers was characterized by the absorption value at their first absorption peak. The three absorption values of the NN monolayers were 8.2×10^{-3}, 5.9×10^{-3}, and 5.0×10^{-3}. A reference sample of the two PE bilayers was also characterised. The absorption measurements of the samples were carried out using a UV-Vis Spectrometer (Shimadzu UV-2401 PC) over the range of 300-800 nm.

Cell line and culture

The human lung-derived A549 cancer cell line was purchased from ATCC (American Tissue Culture Collection, Rockville, MD). A549 were grown in supplemented DMEM medium (Gibco/Invitrogen, La Jolla, CA) containing 4.5 g L^{-1} glucose, 10% Fetal Bovine Serum (FBS), and 5 mg L^{-1} gentamicin in the incubator at 37 °C supplied with 5% CO_2.

Cell viability and NN cell accumulation assessments

The A549 cells were seeded in 96-well plates in 100 µL supplement DMEM containing 10% of FBS and 5 µg/ml gentamicin at 37 °C, 5% CO_2, 90% relative humidity for 24 h. Cell density was 5×10^3 cells/well. In our previous work, [9] it has been shown that quantum dots with cysteine on the surface can lose colloidal stability in the cell culturing medium due to the salt content, and preincubation of the nanoparticles with bovine serum albumin (BSA) imparts particle stability. Therefore, NNs were incubated with overnight with 0.3 mg mL^{-1} of BSA, which is average concentration of BSA commonly used cell medium with 10% FBS. Then, NNs mixed with DMEM containing 10% FBS were added to cells and incubated at 37 °C for 24 h. The NN concentration used for the cytotoxicity assay was 20 µg/ml, and for NN cell accumulation test it ranged from 10-80 µg/ml. The volume of maximum addition was 10 µL per well (10% of medium volume). After fixation in 3.7% formaldehyde for 30 min, the cellular nuclei were stained with Hoechst 33432 dye. Cell imaging and recording were carried out using Cytell Cell Imaging System (GE Healthcare, Buckinghamshire, UK). Cell viability was estimated by the preinstalled GE Cell Viability BioApp 2-color protocol at 10x magnification. Ten random fields were imaged across the entire well area of each NN concentration exposure point. Exposures were repeated three times. Average cell viability was calculated comparing data from experimental samples and negative control. Positive control was 100 µM valinomycin as indicated.

Instrumentation

UV-Vis absorption spectroscopy studies were carried out using a Varian Cary 60 UV-visible spectrophotometer, and a Shimadzu UV-2401 PC spctrophotomter. PL characterization was carried out using a Horiba Jobin Yvon Fluorolog-3 using a Hamamastu InP/InGaAs photomultiplier (R5509-7-3). The excitation wavelength used for the PL measurements was performed at least 20 nm below the emission range. Photoluminescent quantum yields (PLQY) were measured using the comparison approach using Rhodamine 6G in ethanol (PLQY = 95%) as a standard. Circular Dichroism (CD) Spectroscopy was carried out using a Jasco J-815 CD spectrometer operating under a N_2 flow of 5-8 L/min. Transmission Electron Microscopy (TEM) was performed using a FEI Titan electron microscope operating at a beam voltage of 300 kV, while the same instrument was used to carry out scanning transmission electron microscopy (STEM) high-angle annular dark-field imaging (HAADF) and EDX analysis. Photoluminescence lifetime measurements were performed using a time-correlated single photon counting (TCSPC) spectrometer equipped with a PCS900 plug-in PC card (Fluorolog-3 Horiba Jobin Yvon) and a semiconductor diode "NanoLED" excitation source (458 nm, Horiba Jobin Yvon) with pulse duration shorter than 1 ns. Lifetimes were obtained by a reconvolution fit using a solution of Ludox in water as the scatterer and the quality of fit judged by minimization of reduced chi-squared and the residuals. Time resolved photoluminescence (TRPL) measurements were obtained using a PicoQuant Microtime200 time-resolved confocal microscope system with 100 ps resolution. The TRPL spectra were recorded using a single-photon avalanche diode with a x40 objective. The NN QDs were excited by a 10 MHz 405 nm picosecond pulse laser. Measurements were done over an area of 80 x 80 μm^2 and an integration time of 4 ms. A narrow-band filter at 600 nm and a broadband filter at 650 nm were used to measure the blue and red sides of the NN QD monolayer emission. TRPL measurements of the overall emission was also measured without filtering any of the emission. The PL spectra were measured under the same excitation conditions as the TRPL and recorded using an Andor Shamrock sr-303i spectrometer with an Andor Newton 970EMCCD. The PL data was recorded over an area of 80 µm x 80 µm and an integration time of 3.8 ms. All measurements were done at room temperature.

II. Zinc Blende CdSe QD Data

Table S1. Synthetic conditions used for zb-CdSe QD seed synthesis.

Sample Name	Injection Temperature (˚C)	Growth Temperature (˚C)	Growth Time (min)	Scale of reaction
zb-CdSe-1	240	240	0	1
zb-CdSe-2	240	240	0	0.5
zb-CdSe-3	240	240	2	1
zb-CdSe-4	240	240	3	0.5

Table S2. Parameters calculated from absorption and emission spectra of zb-CdSe QD seeds.

Sample Name	1st Exciton Absorption position (nm)	HWHM (nm)	HWHM(eV)	Diameter (nm)	PL peak (nm)	Stokes shift	FWHM (nm)
zb-CdSe-1	475.5	17.5	9.26×10^{-2}	2.1	480	4.5	42
zb-CdSe-2	488.5	18.5	9.267×10^{-2}	2.24	493.5	5	31.5
zb-CdSe-3	549.0	14.5	5.80×10^{-2}	3.0	556	6.5	32
zb-CdSe-4	574.5	15.5	5.67×10^{-2}	3.65	582	8	33

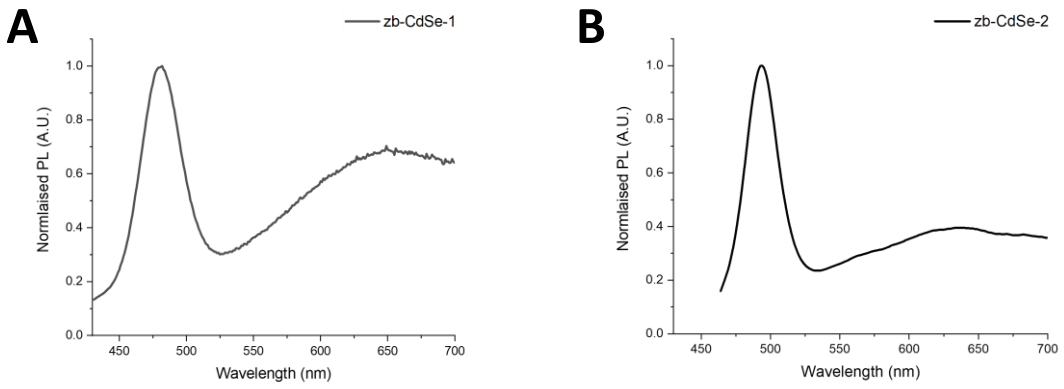

Fig. S1. PL spectra of zb-CdSe-1 (A) and zb-CdSe-2 (B) showing the excitonic and the large broad surface defect emission.

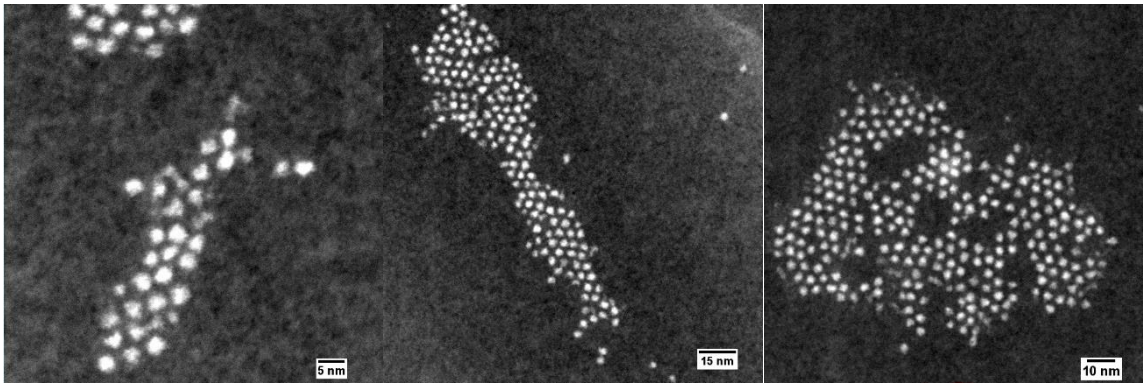

Fig. S2. STEM images of sample zb-CdSe-2.

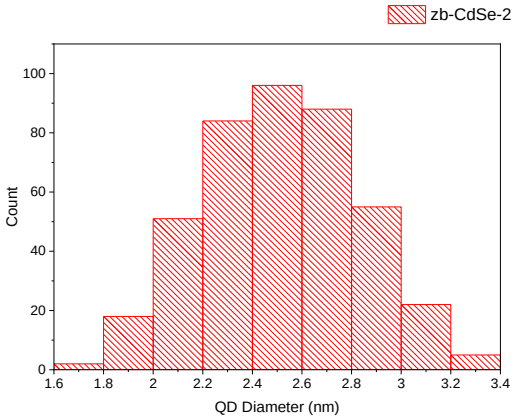

Fig. S3. Histogram of size distribution of sample zb-CdSe-2, giving a mean = 2.52 +/-0.31 nm using n=421 measurements.

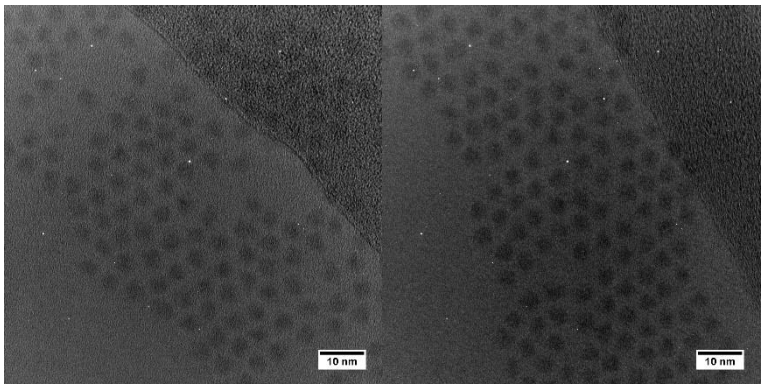

Fig. S4. Additional TEM images of sample zb-CdSe-4.

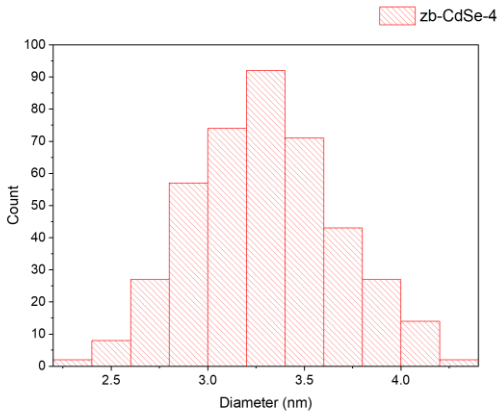

Fig. S5. Histogram of size distribution of sample zb-CdS- 4, giving a mean = 3.3 +/-0.38 nm using n=418 measurements.

III. Synthetic Conditions for Synthesis of Nanonail CdSe/CdS Structures

Table S3. Experimental conditions used for CdSe/CdS NN synthesis.

Sample Name	Core (seed) used	Diameter of core (nm)	Amount of seeds used (nmol)	Core to shell ratio relative to original
CdSe/CdS NN-1	zb-CdSe-1	2.1	15	2
CdSe/CdS NN-2	zb-CdSe-2	2.25	15	2
CdSe/CdS NN-3	zb-CdSe-3	2.9	15	2
CdSe/CdS NN-4	zb-CdSe-4	3.65	15	2
CdSe/CdS NN-5	zb-CdSe-2	2.25	7.5	1
CdSe/CdS NN-6	zb-CdSe-3	2.9	7.5	1
CdSe/CdS NN-7	zb-CdSe-4	3.65	7.5	1

IV. Electron Microscopy Characterisation of Nanonail Structures

Table S4. Dimensions of CdSe/CdS NNs samples, as measured from TEM images. Uncertainties in aspect ratios and tapering ratios were calculated using error propagation from the standard deviations in measured lengths and widths of the NNs.

Sample Name	Length (nm)	Width (top) (nm)	Width (end) (nm)	Aspect ratio (end width)	Aspect Ratio (top width)	Tapering Ratio (end AR/top AR)
CdSe/CdS NN-1	44.7 ± 7.7	10.9 ± 1.3	7.2 ± 0.9	6.2 ± 1.3	4.1 ± 0.9	1.5 ± 0.5
CdSe/CdS NN-2	56.8 ± 10.5	13.3 ± 1.9	7.0 ± 0.9	8.1 ± 1.8	4.3 ± 1.0	1.9 ± 0.6
CdSe/CdS NN-3	65.9 ± 14.6	12.0 ± 2.1	5.4 ± 0.7	12 ± 3.1	5.5 ± 1.6	2.2 ± 0.8
CdSe/CdS NN-4	23.9 ± 6.1	10.0 ± 1.5	6.8 ± 1.3	3.5 ± 1.1	2.4 ± 0.7	1.5 ± 0.6
CdSe/CdS NN-5	38.8 ± 5.7	10.0 ± 1.4	5.8 ± 0.9	6.7 ± 1.4	3.9 ± 0.8	1.7 ± 0.5
CdSe/CdS NN-6	44.2 ± 7.6	12.1 ± 2.0	6.6 ± 0.9	6.7 ± 1.5	3.6 ± 0.9	1.8 ± 0.6
CdSe/CdS NN-7	39.6 ± 7.1	10.8 ± 1.6	6.2 ± 0.8	6.4 ± 1.4	3.7 ± 0.9	1.7 ± 0.6

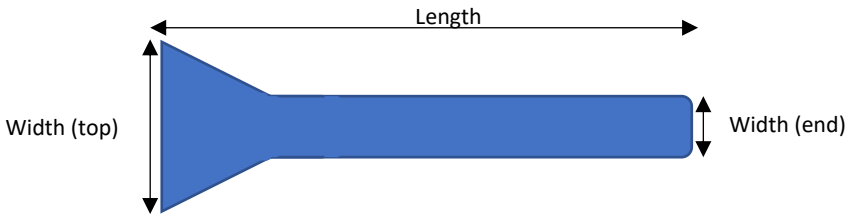

Fig. S6. Schematic demonstrating how dimensions were obtained from measurements of TEM images.

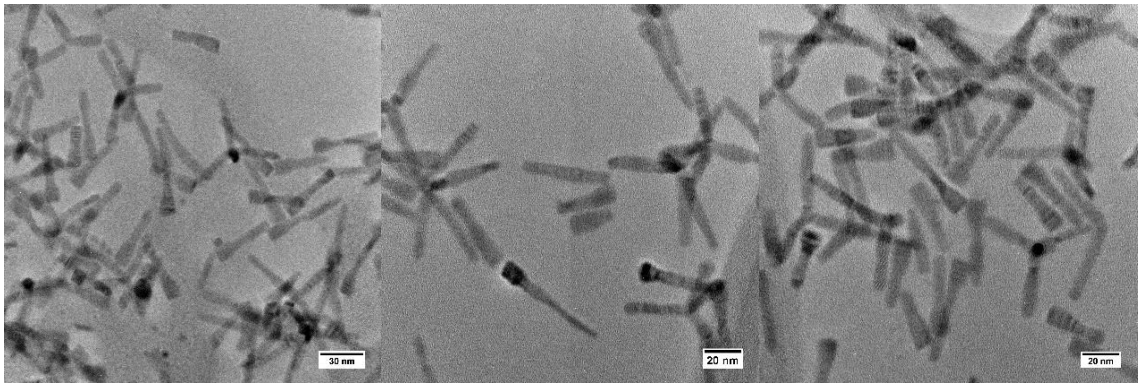

Fig. S7. Representative TEM of CdSe/CdS NN-1.

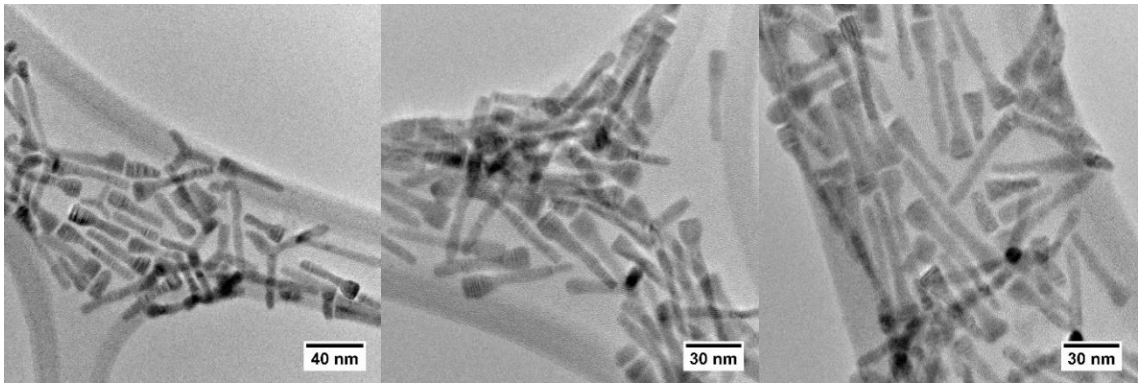

Fig. S8. Representative TEM of CdSe/CdS NN-2.

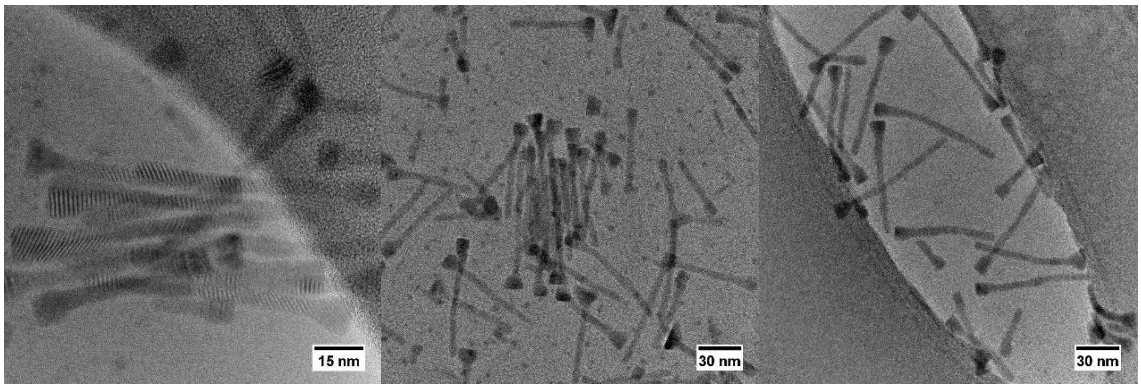

Fig. S9. Representative TEM of CdSe/CdS NN-3.

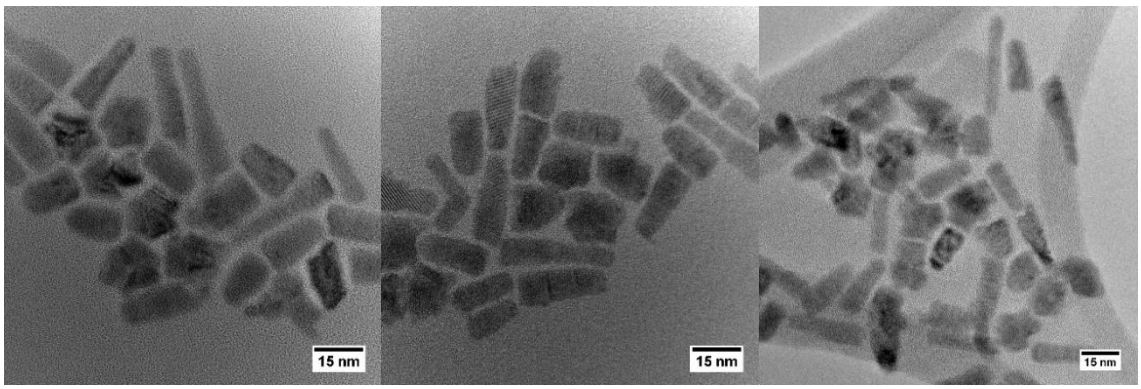

Fig. S10. Representative TEM of CdSe/CdS NN-4.

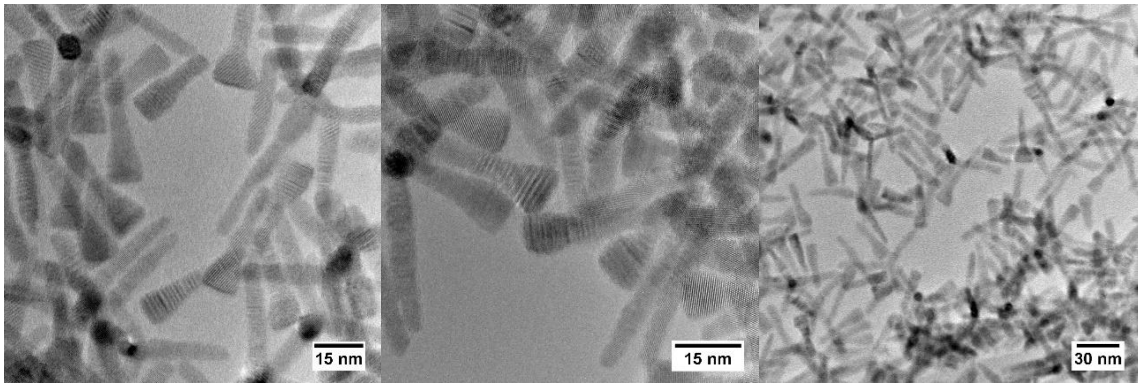

Fig. S11. Representative TEM of CdSe/CdS NN-5.

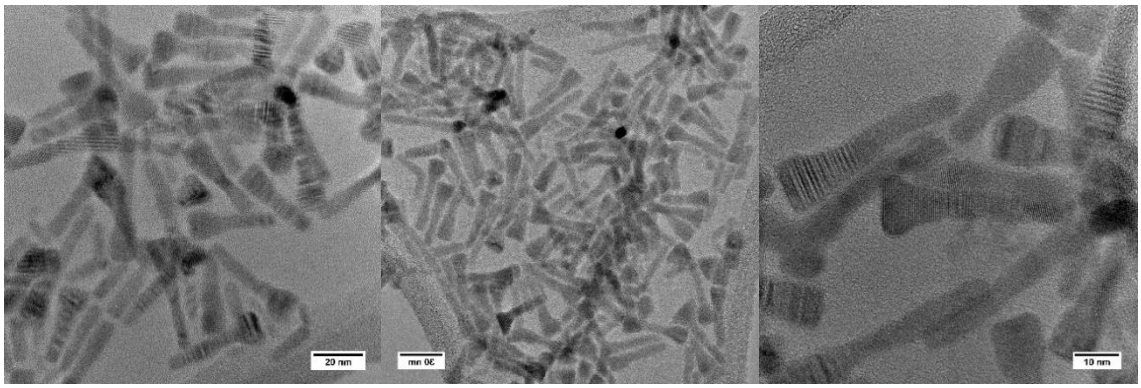

Fig. S12. Representative TEM of CdSe/CdS NN-6.

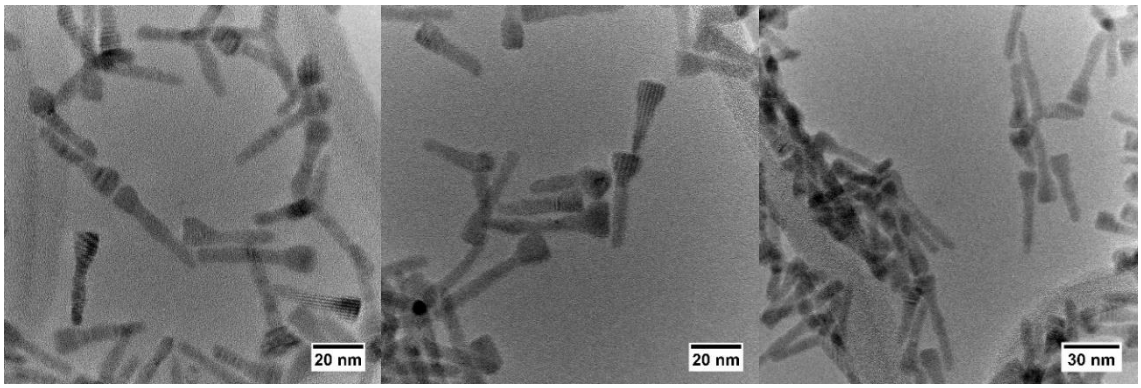

Fig. S13. Representative TEM of CdSe/CdS NN-7.

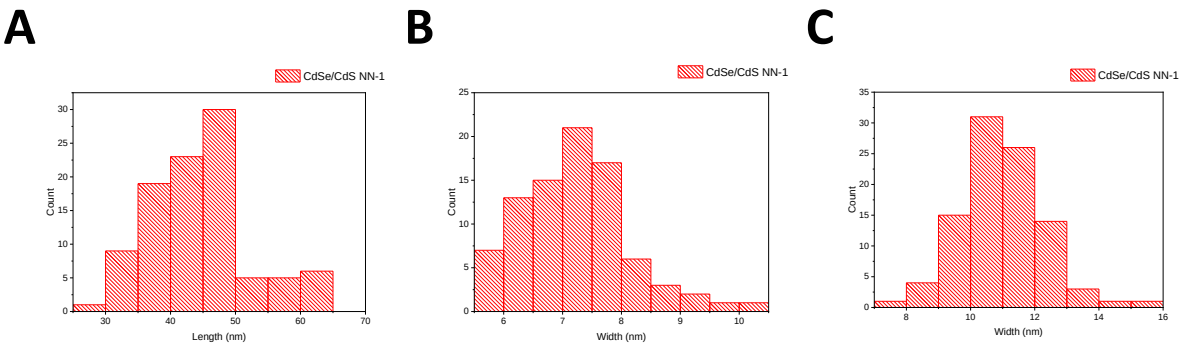

Fig. S14. Histogram of distribution of CdSe/CdS NN-1, with measurements taken of the length (A)= 44.7±7.7 nm, width (end) (B)=7.2±0.9 nm and width (top) (C)=10.9±1.3 nm.

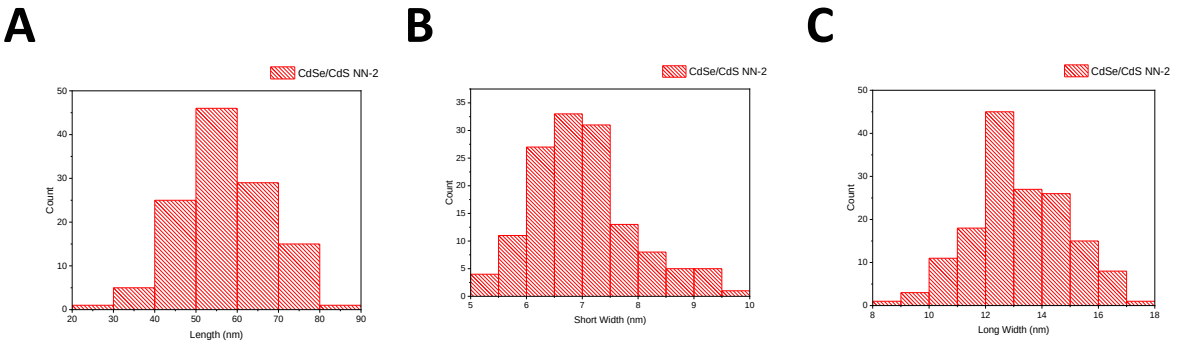

Fig. S15. Histogram of distribution of CdSe/CdS NN-2, with measurements taken of the length (A)= 56.8±10.5 nm, width (end) (B)=7.0±0.9 nm and width (top) (C)=13.3±1.9 nm.

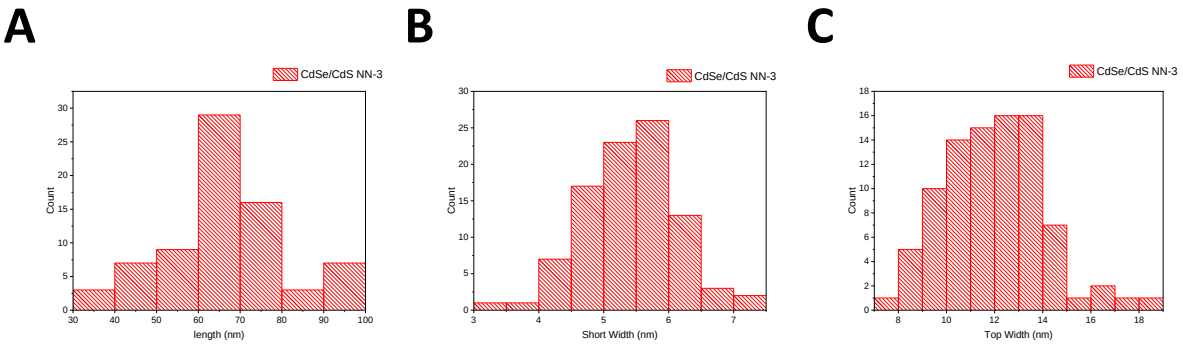

Fig. S16. Histogram of distribution of CdSe/CdS NN-3, with measurements taken of the length (A)= 65.9±14.6 nm, width (end) (B)=5.4±0.7 nm and width (top) (C)=12.0±2.1 nm.

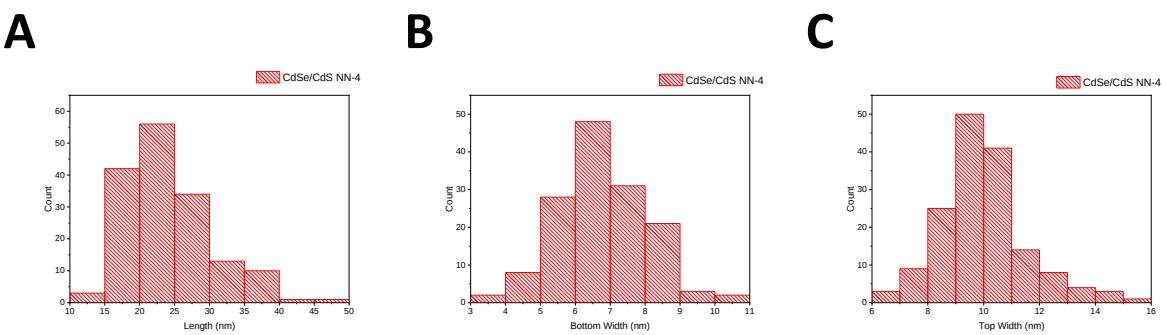

Fig. S17. Histogram of distribution of CdSe/CdS NN-4, with measurements taken of the length (A)= 23.9±6.1 nm, width (end) (B)=6.8±0.9 nm and width (top) (C)=10.0±1.5 nm.

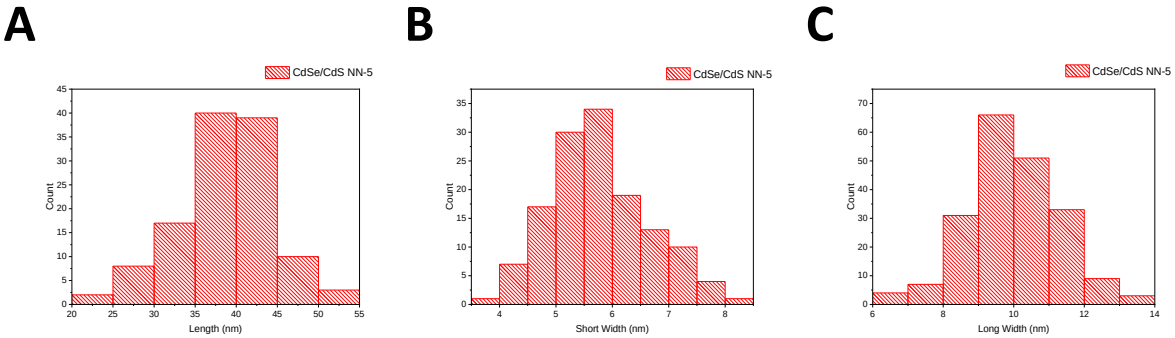

Fig. S18. Histogram of distribution of CdSe/CdS NN-5, with measurements taken of the length (A)= 38.8±5.7 nm, width (end) (B)=5.8±0.9 nm and width (top) (C)=10.0±1.4 nm.

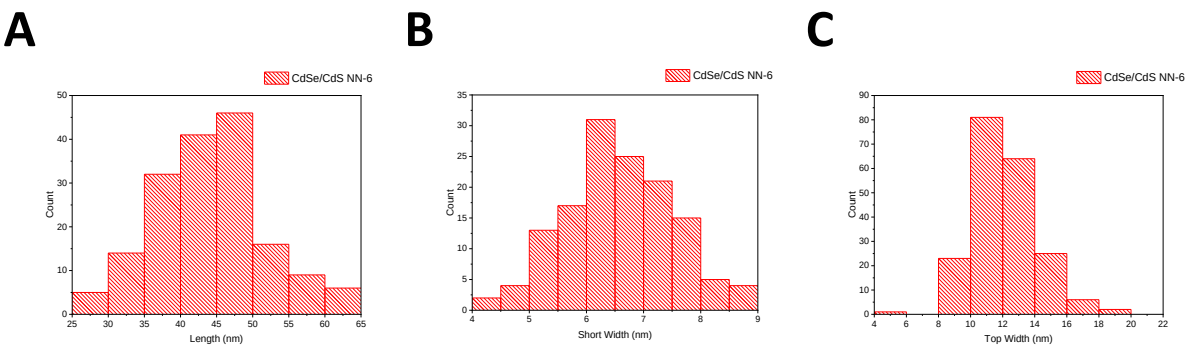

Fig. S19. Histogram of distribution of CdSe/CdS NN-6, with measurements taken of the length (A)= 44.2±7.6 nm, width (end) (B)=6.6±0.9 nm and width (top) (C)=12.1±2.0 nm.

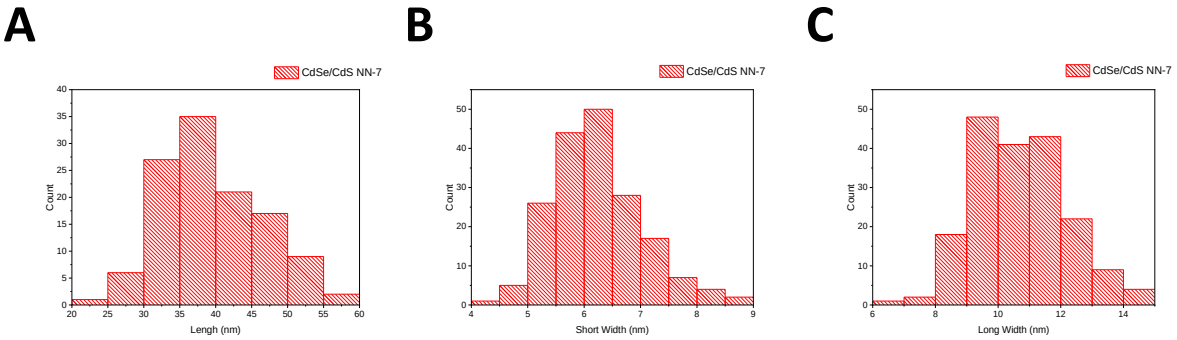

Fig. S20. Histogram of distribution of CdSe/CdS NN-7, with measurements taken of the length (A)= 39.6.2±7.1 nm, width (end) (B)=6.2±0.8 nm and width (top) (C)=10.8±1.6 nm.

V. Optical Characterisation of CdSe/CdS Nanonail Structures

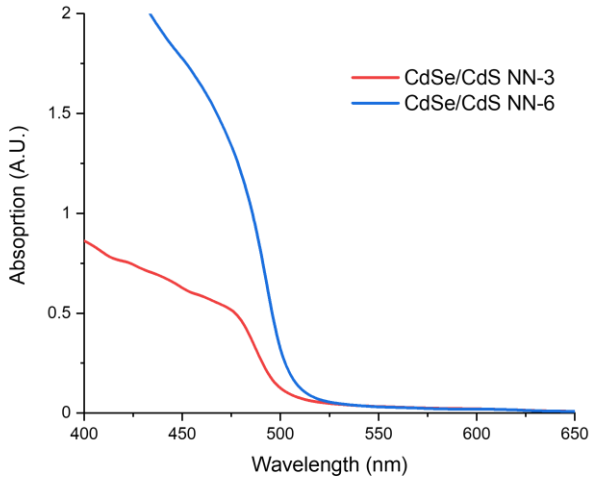

Fig. S21. Absorption spectra of CdSe/CdS NN 3 and 6 , normalised to CdSe absorption peak.

Table S5. Optical properties of CdSe/CdS NN samples.

Sample Name	First exciton position (nm)	First exciton position of core (nm)	PL peak (nm)	FWHM (eV)	PLQY (%)
CdSe/CdS NN-1	475	not clear	multiple, 599.5	-	Below 0.1
CdSe/CdS NN-2	488.5	not clear, 590	601	0.154	Below 0.1
CdSe/CdS NN-3	545	not clear, 602	621.5	0.102	1.6 +/- 0.16
CdSe/CdS NN-4	574.5	620	633	0.09	19.0 +/- 1.9
CdSe/CdS NN-5	488.5	not clear, 600	597	0.15	1.0 +/- 0.1
CdSe/CdS NN-6	545	604.5	612.5	0.102	13.2 +/- 1.3
CdSe/CdS NN-7	574.5	621	629	0.088	0.7 +/- 0.07

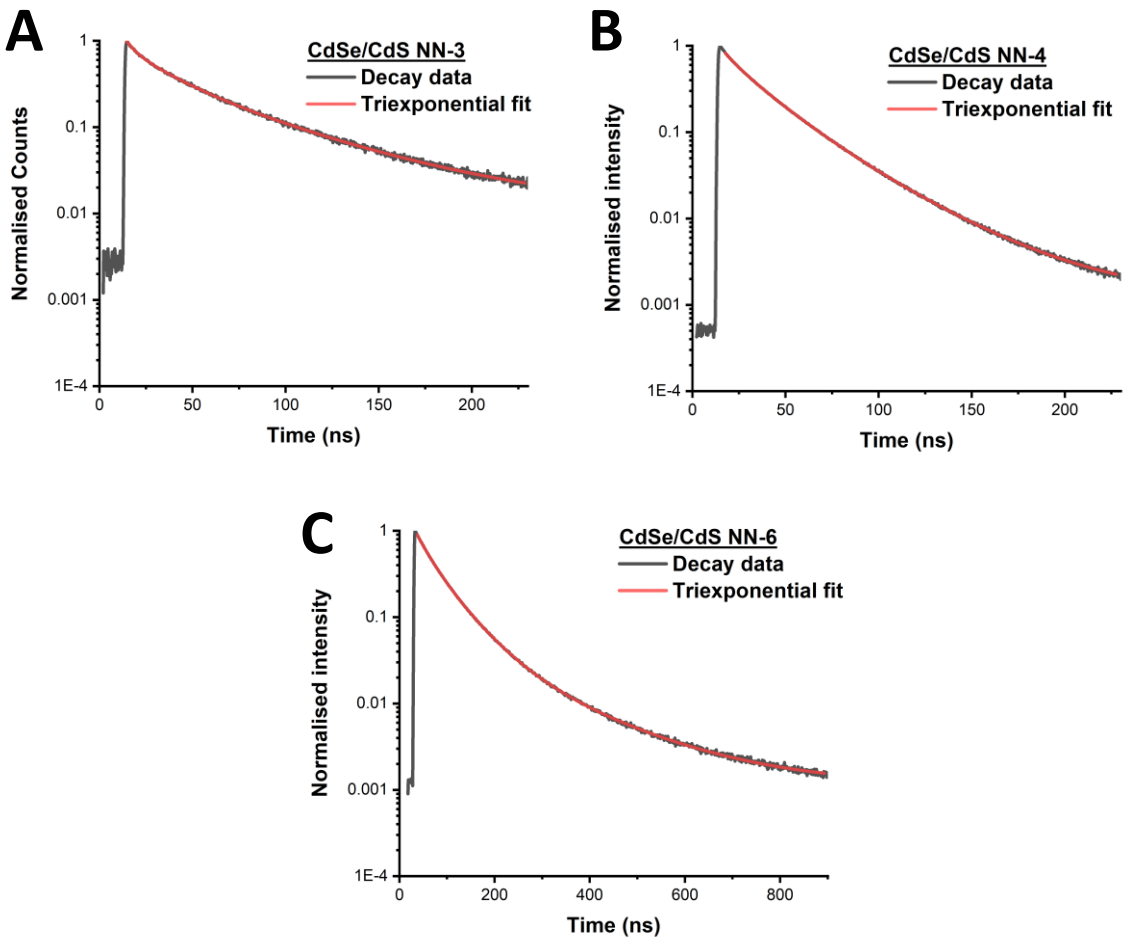

Fig. S22. PL decay graphs of (A) CdSe/CdS NN-3, (B) NN-4, and (C) NN-6.

Table S6. Luminescent lifetimes and fitting parameters from triexponential model for PL decay of CdSe/CdS NN samples.

Sample Name	t_{avg} (ns)	t_1 (ns)	Amplitude	t_2 (ns)	Amplitude	t_3 (ns)	Amplitude
CdSe/CdS NN-3	48.2	22.0	27.61	60.6	69.30	4.77	3.09
CdSe/CdS NN-4	27.8	6.38	3.64	20.3	53.62	39.0	42.74
CdSe/CdS NN-6	69.6	26.7	23.2	58.5	60.62	173	16.18

Excitation-Emission Matrix

Correction Factor Applied

The correction factor (C_f) considers the absorption at excitation (A_{ex}) and the emission wavelength (A_{em}), and can be calculated using Equation S1. Using this correction factor, it is possible to convert measured intensity (I_{obs}) to corrected intensity (I_c), according to Equation S2.

$$C_f = 10^{\frac{(A_{ex}+A_{em})}{2}} \quad \text{(S1)}$$

$$I_c = I_{obs} \times C_f \quad \text{(S2)}$$

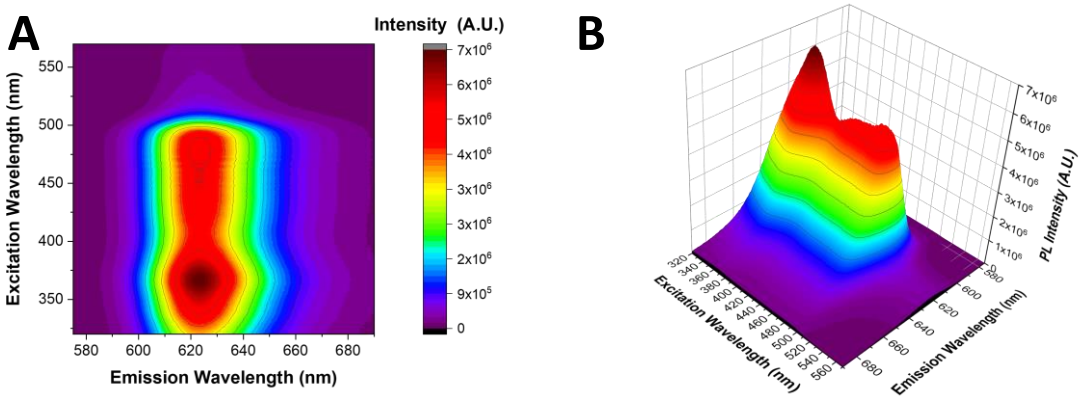

Fig. S23. EEM of CdSe/CdS NN-6 shown in a contour map (A) and 3-dimensional plot (B) using the uncorrected data.

VI. CdSe/CdS Dot in Tetrapods

Methods

zb-CdSe using Se-ODE

This is a modified method from literature. [10, 11] Firstly, 0.5 mmol/mL of $Cd(OA)_2$ (0.0642 g/ml) solution was prepared by reacting 5 mmol (0.642 g) of CdO, 5 mL of OA , and 5 mL of ODE. The solution was degassed for 30 minutes at 30 °C. The mixture was heated to 280 °C under N_2 flow for 20 min. After the mixture was optically clear, it was cooled down to 50 °C. Next, 1 mmol of Se (0.078 g) and 10 mL of ODE (7.9 g) were loaded into a 100 mL 3-neck round flask and, degassed for 30 minutes and then heated up to (300 -320 °C) under Ar. When the Se/ ODE solution become optically clear, 2 mmol of Cd $(oleate)_2$ solution (4 mL) was rapidly injected into the solution and reacted at (270-300 °C) for 15 min. Finally, the solution was cooled to room temperature. This crude solution was used without purification for the next step in the synthesis.

Table S7. Experimental conditions used for zb-CdSe QD synthesis using Se-ODE

Sample Name	Injection Temperature (˚C)	Growth Temperature (˚C)	First Exciton Position (nm)	Estimation of size from UV-Vis (nm)
zb-CdSe-5	300	270	620	5.6
zb-CdSe-6	320	300	585	4.0

Table S8. Experimental conditions used for zb-CdSe QD synthesis using Se-ODE

Sample Name	CdSe Seeds used	Injection temperature (˚C)
CdSe/CdS DiT 1	zb-CdSe-5	350
CdSe/CdS DiT 2	zb-CdSe-6	350

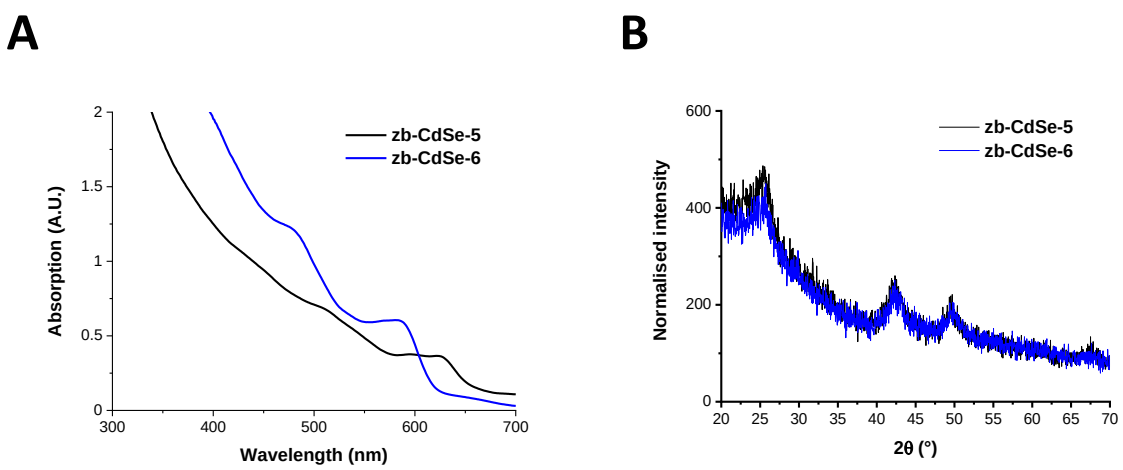

Fig. S24. UV-Vis (A) and XRD (B) of the two CdSe QD samples produced using Se-ODE as a Se source.

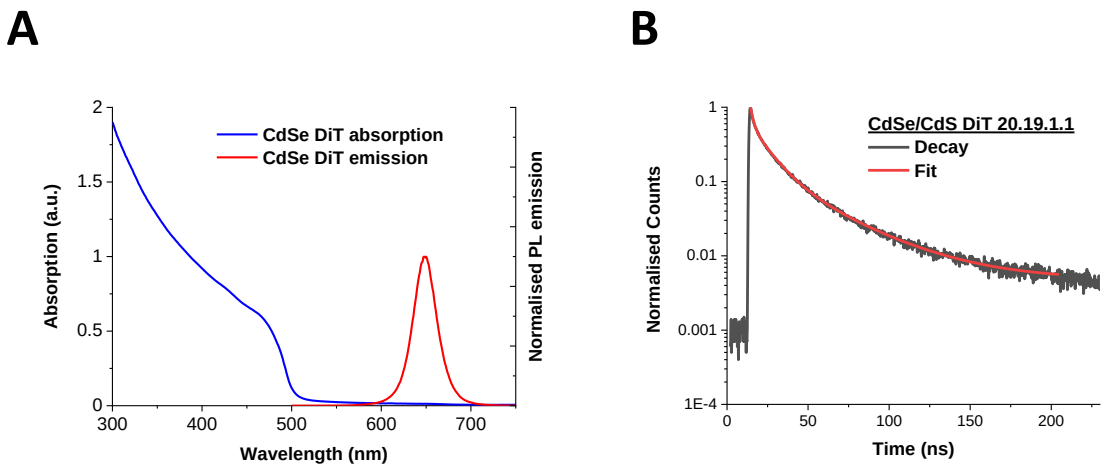

Fig. S25. PL and UV-Vis (A) and Pl decay (B) of CdSe/CdS DiT

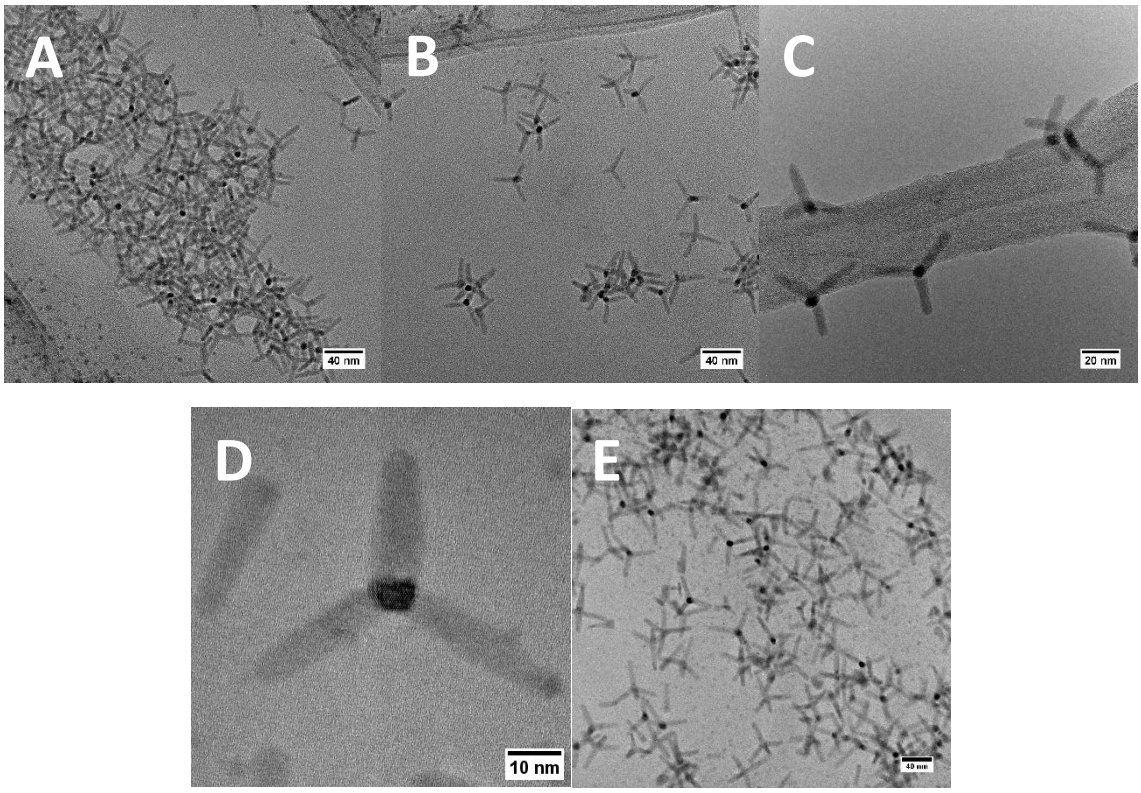

Fig. S26. Representative TEM images of CdSe/CdS DiTs.

Table S9. Luminescent lifetimes and fitting parameters from triexponential model for PL decay of CdSe/CdS DiT sample.

Sample Name	t_{avg} (ns)	t_1 (ns)	Amplitude	t_2 (ns)	Amplitude	t_3 (ns)	Amplitude
CdSe/CdS DiT 1	22.8	11.2	45.39	36.9	47.80	1.73	6.80

VII. Spectroscopic Studies of Chiral CdSe/CdS NNs and Cellular Uptake of Chiral CdSe/CdS spherical QDs

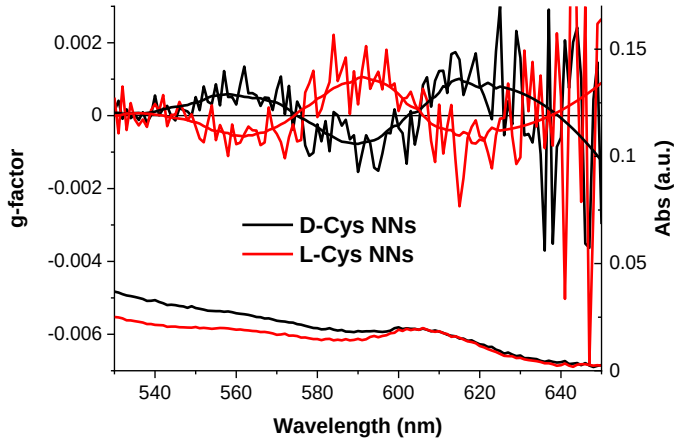

Fig. S27. g-factor spectra of L- and D-Cys CdSe/CdS NNs in the CdSe core absorption region, with both raw and smoothed data presented.

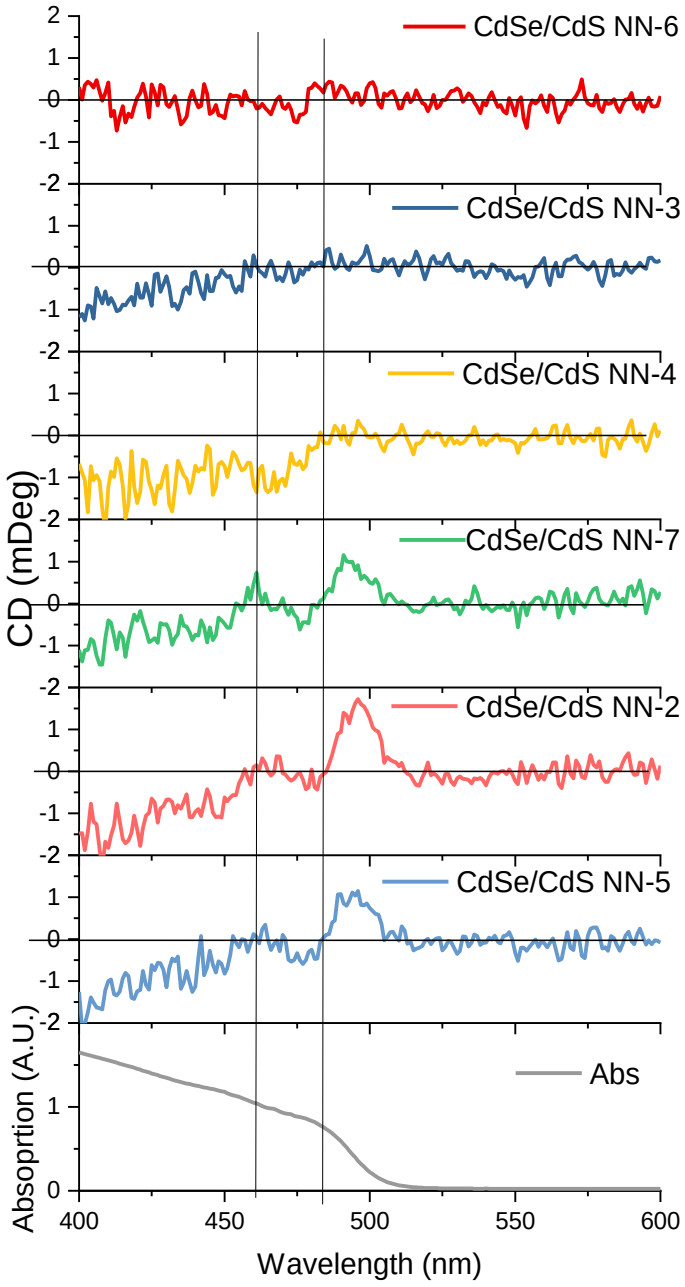

Fig. S28. CD spectra of CdSe/CdS NN samples after ligand exchange with L-Cys.

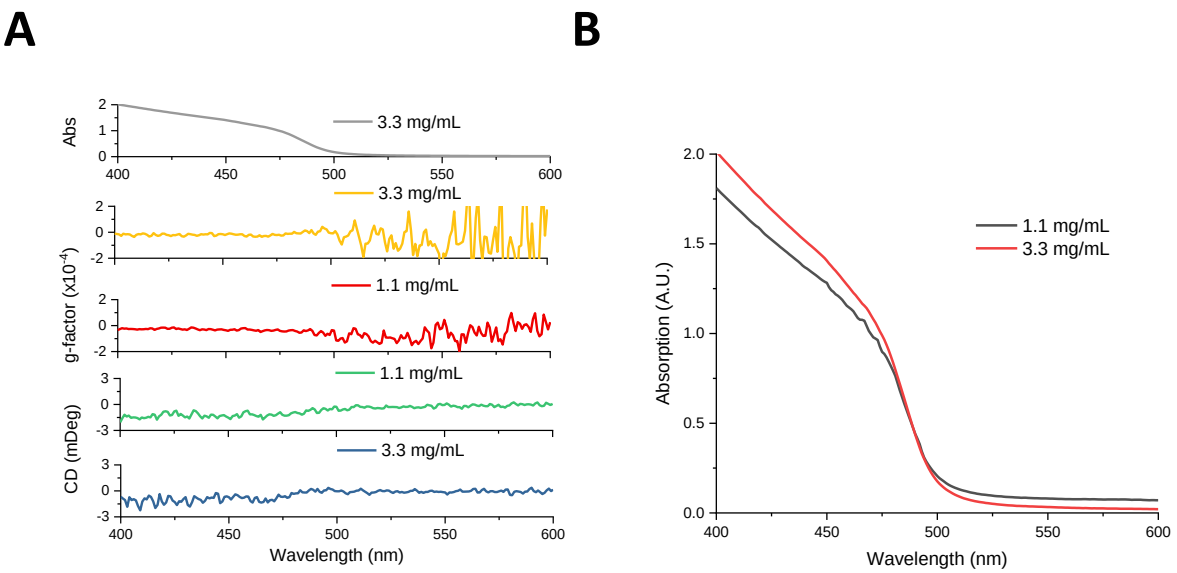

Fig. S29. CD spectra and g-factor for CdSe/CdS NN-4 (A) and UV-Vis absorption (B) measured using two concentrations of cysteine ligand (1.1 and 3.3 mg/mL).

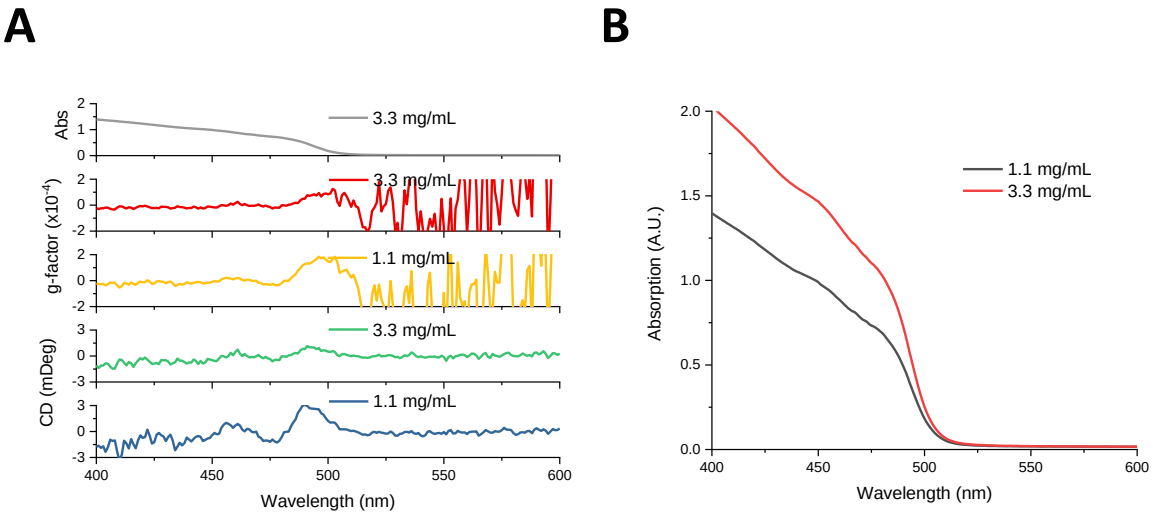

Fig. S30. CD spectra and g-factor for CdSe/CdS NN-7 (A) and UV-Vis absorption (B) measured using two concentrations of cysteine ligand (1.1 and 3.3 mg/mL).

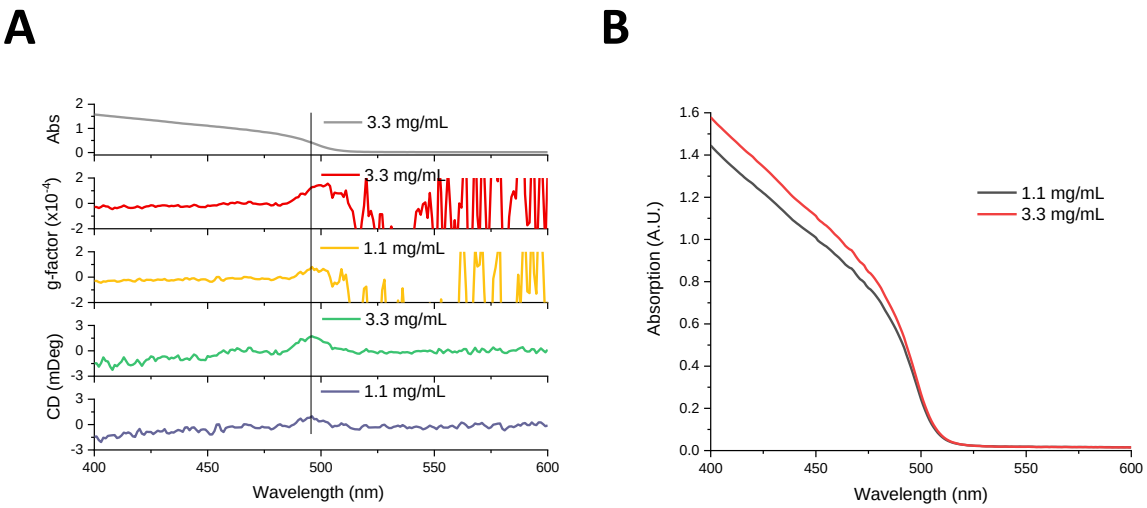

Fig. S31. CD spectra and g-factor for CdSe/CdS NN-2 (A) and UV-Vis absorption (B) measured using two concentrations of cysteine ligand (1.1 and 3.3 mg/mL).

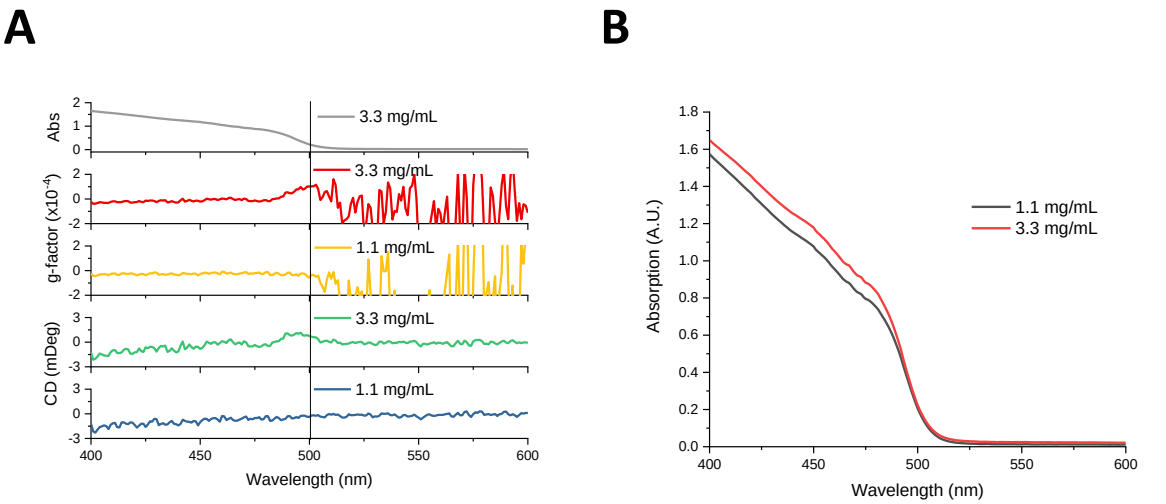

Fig. S32. CD spectra and g-factor for CdSe/CdS NN-5 (A) and UV-Vis absorption (B) measured using two concentrations of cysteine ligand (1.1 and 3.3 mg/mL).

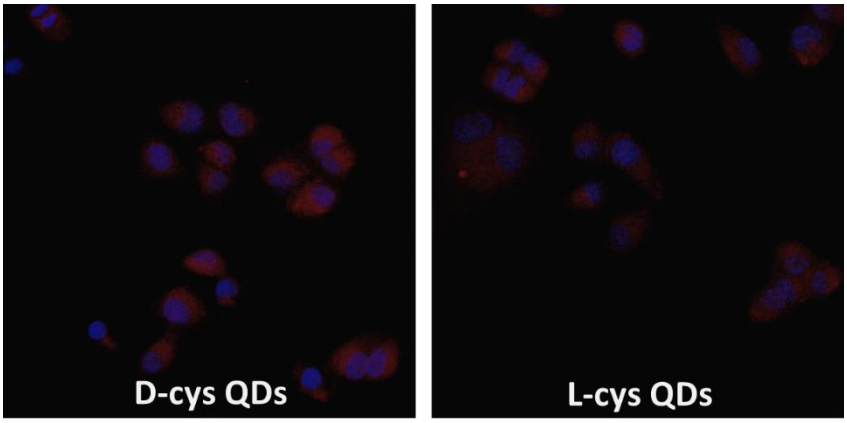

Fig. S33. PL images of A549 cells incubated with L- Cys and D- Cys spherical quantum dots for 24 h.

VIII. Energy Transfer in NN Monolayers

Results: Monolayers of NNs by LBL

NNs in Solution

The PL (dashed line) and absorption (solid line) spectra of CdSe/CdS NN-3 in aqueous solution and in monolayers are shown in Fig. S34B. The NNs in solution have a PL emission peak at approximately 620 nm with a full width at half maximum (FWHM) of 31 nm. The first absorption peak is at approximately 464 nm.

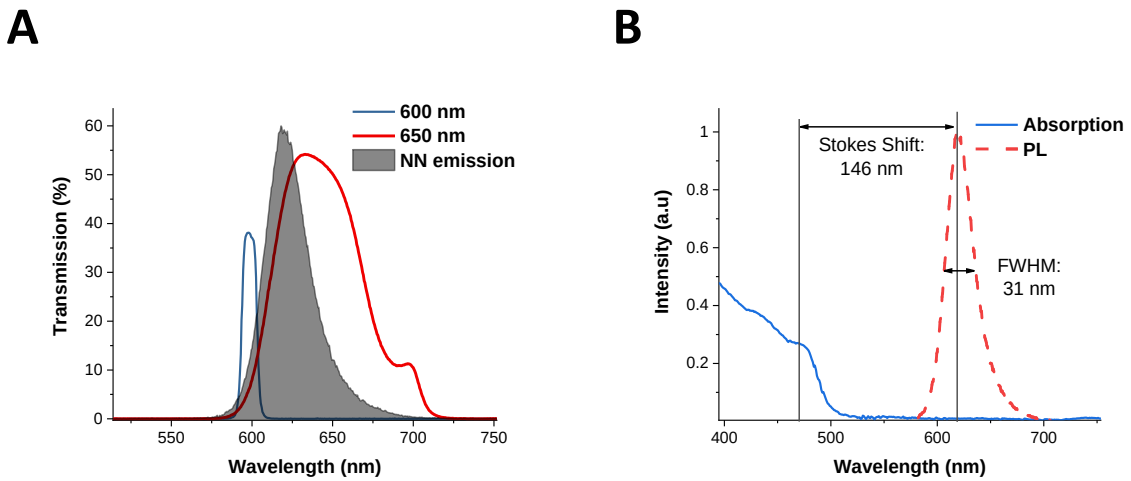

Fig. S34. (A) Transmission spectra of the 600 nm narrow-band filter (blue) and the 650 nm broadband filter (red). (B) Absorption and PL spectra of CdSe/CdS NN-3 in aqueous solution.

NN PL in monolayers

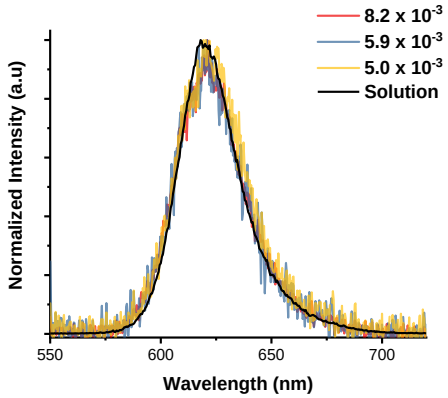

Fig. S35. Normalized PL spectra of CdSe/CdS NN-3 in monolayers of varying concentration monolayers and solution. Note, each concentration is given as its UV-Vis absorbance at 464 nm.

NN PL decay in monolayers

The PL decays measured using the 600 nm filter are shown in Fig. S35. Each decay was fit using a biexponential function, and the average lifetime was extracted according to Equation S3.

$$\tau_{avg} = \frac{A\tau_1^2+B\tau_2^2}{A\tau_1+B\tau_2}. \quad \text{S3}$$

The measurements were performed at a number of positions across the sample with a variation of approximately 10%, represented as the error in the data points in Fig. S36.

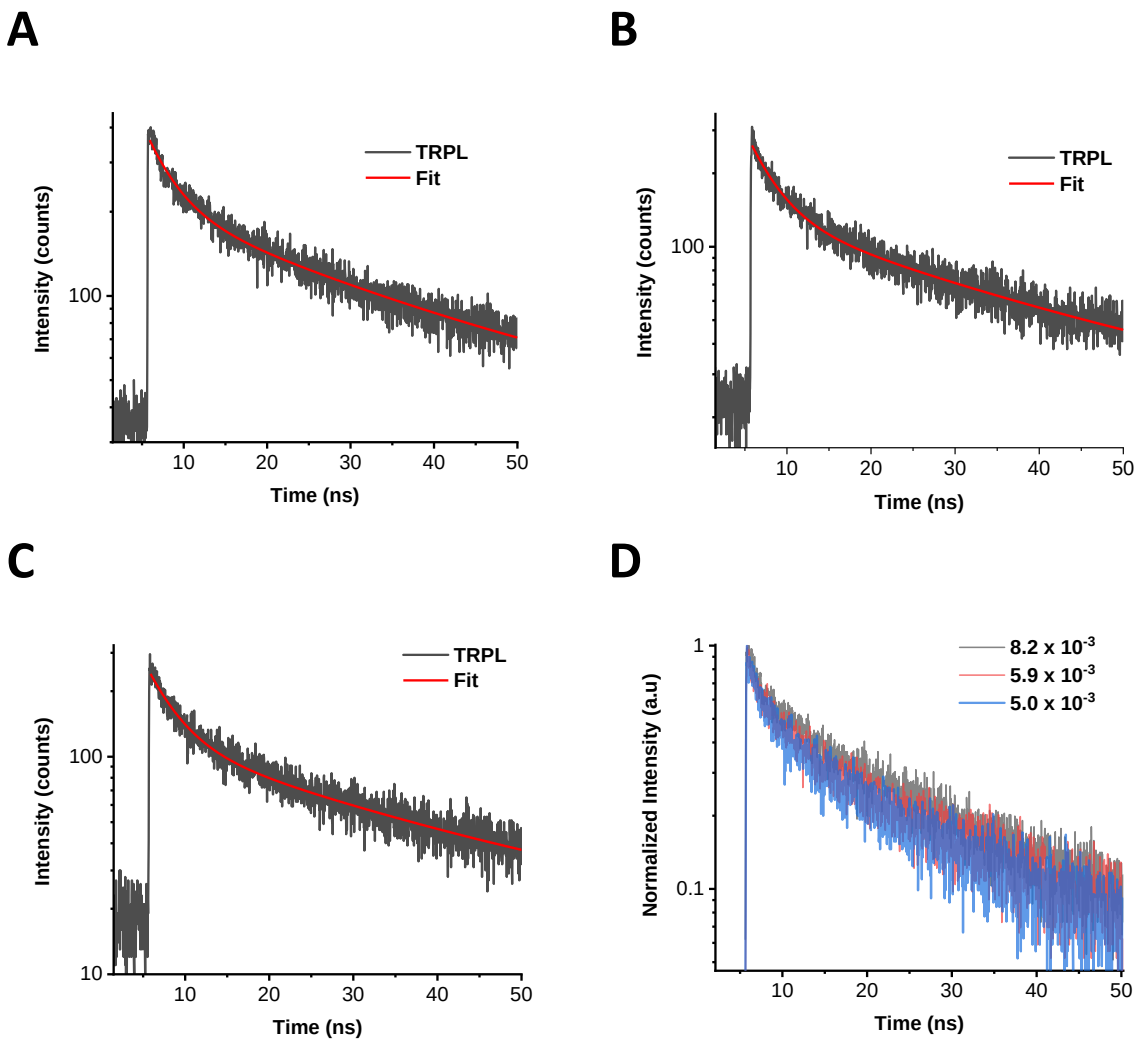

Fig. S36. TRPL and bi-exponential fits of CdSe/CdS NN-3 measured with 600 nm filter for monolayers of concentration (A) abs = 8.2 x 10^{-3} , (B) abs = 5.9 x 10^{-3} , (C) abs = 5.0 x 10^{-3} . (D) Normalized TRPL of the three different monolayers.

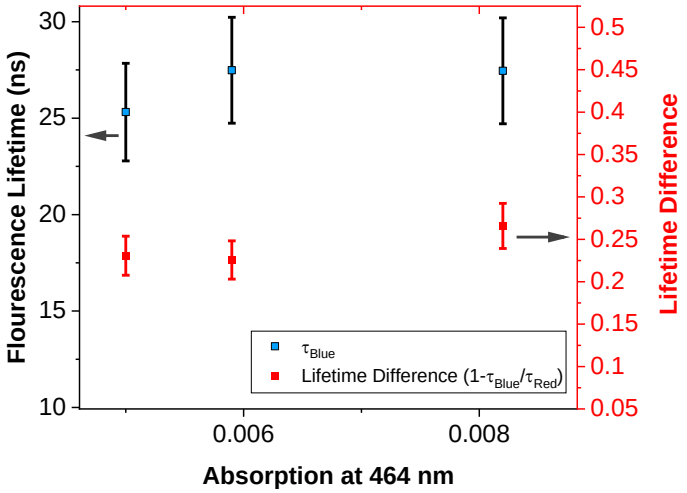

Fig. S37. Average fluorescence decay lifetimes of NN monolayers of τ_{Blue} (measured with 600 nm filter) and $1\text{-}\tau_{Bue}/\tau_{Red.}$

Relevant Background Theory

Due to the size distribution within QD ensembles, smaller QDs can transfer energy non-radiatively to larger quantum dots. The non-radiative energy transfer affects the emission properties of the QDs, inducing a red shift of the emission peak and decrease in the fluorescence.[5] Förster resonant energy transfer (FRET) has been previously observed and reported in assemblies of QDs.

FRET is a non-radiative energy transfer mechanism between an excited donor (D) to an acceptor (A). FRET is a dipole-dipole interaction and therefore strongly dependant on the separation of the D and A. It is also depends on the spectral overlap of the donor emission and the acceptor absorption. [12, 13] [14] The FRET rate for a D-A pair is given by Equation S4:

$$k_{FRET} = \frac{1}{\tau_D}\left(\frac{R_0^6}{r_{DA}^6}\right) \quad \text{S4}$$

where τ_D is the donor lifetime, R_0 is the Förster radius, and r_{DA} is the separation between donor and acceptor. The Förster radius is the separation distance at which the FRET efficiency is at 50% and it is given by Equation S5:

$$R_0^6 = \frac{9(\ln 10)\kappa^2 \phi_D J(\lambda)}{128\pi^5 n^4 N_A} \quad \text{S5}$$

where κ^2 is the orientation factor, ϕ_D is the quantum efficiency of the donor, N_A is Avogadro's number, n is the refractive index of the medium, and $J(\lambda)$ is the overlap integral, which is the degree of overlap between the extinction of the acceptor and the emission of the donor. $J(\lambda)$ can be defined according to Equation S6:

$$J(\lambda) = \int_0^\infty f_D(\lambda)\varepsilon_A(\lambda)\lambda^4 d\lambda \quad \text{S6}$$

where $f_D(\lambda)$ is the normalized emission spectrum of the donor, $\varepsilon_A(\lambda)$ is the extinction spectrum of the acceptor in $M^{-1}cm^{-1}$, and λ is the wavelength in nm.

The FRET efficiency (E) can be calculated using Equation S7.

$$E = \frac{k_{FRET}}{k_{FRET}+\tau_D^{-1}} \qquad \text{S7}$$

In this work we look at an ensemble of donor and acceptors. The donor can transfer its energy to multiple acceptors and k_{FRET} is the sum of all the individual energy transfer rates k_i to acceptor *i* with donor-acceptor separation r_i, so Equation S4 then becomes:

$$k_{FRET} = \sum_i k_i = \tau_D^{-1} \sum_i \left(\frac{R_0^6}{r_i^6}\right) \qquad \text{S8}$$

Inserting Equation S8 into S7 gives the FRET efficiency for a system of multiple acceptors, according to Equation S9:

$$E = \frac{1}{1+\left(\sum_i \frac{R_0^6}{r_i^6}\right)^{-1}} \qquad \text{S9}$$

Experimentally the FRET efficiency can be determined from spectroscopic data, including the donor fluorescence lifetimes (τ_D and τ_{DA}), and fluorescence intensities, (I_D and I_{DA}) in the absence and presence of the acceptor, respectively, according to Equation S10:

$$E = 1 - \frac{\tau_{DA}}{\tau_D} = 1 - \frac{I_{DA}}{I_D} \qquad \text{S10}$$

In summary, for a size distribution of QDs with a relatively small Stokes shift, the smaller quantum dot emission will overlap with the extinction of the larger QDs, resulting in a non-zero overlap integral J and the possibility for FRET to occur.[5, 15] In these systems, the smaller QDs exhibit a decrease in fluorescence lifetime.[5, 15] FRET from the smaller QDs (contributing to the blue side of the ensemble emission spectrum) to the larger ones (contributing to the red side of the emission spectrum) results in reduced fluorescence lifetime and decreased the emission from the smaller QDs, with increased emission from the larger QDs.

References

1. B. Mahler, P. Spinicelli, S. Buil, X. Quelin, J. P. Hermier and B. Dubertret, *Nature materials*, 2008, **7**, 659-664.
2. M. B. Mohamed, D. Tonti, A. Al-Salman, A. Chemseddine and M. Chergui, *The Journal of Physical Chemistry B*, 2005, **109**, 10533-10537.
3. J. I. Wong, N. Mishra, G. Xing, M. Li, S. Chakrabortty, T. C. Sum, Y. Shi, Y. Chan and H. Y. Yang, *ACS Nano*, 2014, **8**, 2873-2879.
4. M. V. Mukhina, V. G. Maslov, I. V. Korsakov, F. P. Milton, A. Loudon, A. V. Baranov, A. V. Fedorov and Y. K. Gun'ko, 2015.
5. M. Lunz, A. L. Bradley, W.-Y. Chen, V. A. Gerard, S. J. Byrne, Y. K. Gun'ko, V. Lesnyak and N. Gaponik, *Physical Review B*, 2010, **81**, 205316.
6. S. Vial, I. Pastoriza-Santos, J. Pérez-Juste and L. M. Liz-Marzán, *Langmuir*, 2007, **23**, 4606-4611.
7. M. Lunz, A. L. Bradley, W.-Y. Chen and Y. K. Gun'ko, *The Journal of Physical Chemistry C*, 2009, **113**, 3084-3088.
8. G. Decher, *Science*, 1997, **277**, 1232-1237.

9. V. A. Kuznetsova, A. K. Visheratina, A. Ryan, I. V. Martynenko, A. Loudon, C. M. Maguire, F. Purcell-Milton, A. O. Orlova, A. V. Baranov, A. V. Fedorov, A. Prina-Mello, Y. Volkov and Y. K. Gun'Ko, *Chirality*, 2017, **29**, 403-408.
10. J. Lim, W. K. Bae, K. U. Park, L. zur Borg, R. Zentel, S. Lee and K. Char, *Chem. Mat.*, 2012, **25**, 1443-1449.
11. L. Liu, Z. Zhuang, T. Xie, Y.-G. Wang, J. Li, Q. Peng and Y. Li, *J. Am. Chem. Soc.*, 2009, **131**, 16423-16429.
12. J. R. Lakowicz, *Principles of Fluorescence Spectroscopy*, Springer US, 2013.
13. I. L. Medintz and N. Hildebrandt, *FRET - Förster Resonance Energy Transfer: From Theory to Applications*, Wiley, 2013.
14. J. B. Hoffman, H. Choi and P. V. Kamat, *The Journal of Physical Chemistry C*, 2014, **118**, 18453-18461.
15. A. P. Litvin, E. V. Ushakova, P. S. Parfenov, A. V. Fedorov and A. V. Baranov, *The Journal of Physical Chemistry C*, 2014, **118**, 6531-6535.